

Supporting Information for

Non-fluorescent Quantification of Single mRNA with Transient Absorption Microscopy

Jing Liu^{a,b,c}, and Joseph Irudayaraj^{a,1}

^a Department of Agricultural and Biological Engineering, Bindley Bioscience Center, Purdue University, West Lafayette, IN 47907, USA

^b Nanoscience and Nanoengineering, South Dakota School of Mines and Technology, Rapid City, SD 57701, USA.

^c Biochemical Spatio-Temporal NetWork Resource (BioSNTR), State of South Dakota, USA.

This file includes:

Section 1-4.

Figure. S1 to S7.

References (1-8).

¹ To whom corresponding should be addressed: Joseph Irudayaraj, Email: josephi@purdue.edu.

Section 1. Differentiation of AuNPs in Dark-Field Microscopy.

The optical contrast in dark-field microscopy stems from the dielectric mismatch between targets and the environments, resulting in scattering which is proportional to the 6th power of the target size. It is a powerful tool to detect the scattering field of nanosized metal particles, and more information can be obtained by adding a spectrometer for hyper-spectral analysis. However, when detecting metal nanoparticles (NPs), such as AuNPs, in cells, scattering from cell components usually overwhelms the signal from AuNPs or some droplets or lipids that have similar size as the AuNP, leading to similar scattering spectra.

Figure S1 shows a typical darkfield image of MCF-7 cells incubated with 30 nm AuNPs, the imaging scheme was introduced in our previously published works.¹⁻³ We show that it is difficult to identify nanoparticles from the cell components based on the intensity of scattering field without sample preparation steps.⁴ In addition, analysis of the spectrum from different areas marked in Figure S1a suggests that the scattering of cell components can have a significant influence on the localization of AuNPs.

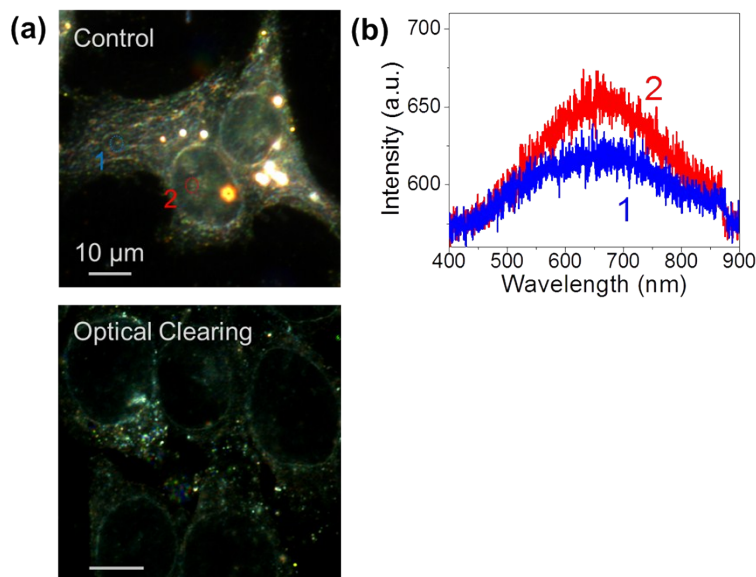


Figure S1. The influence of scattering of cell components on the detection of AuNPs by darkfield microscopy. (a) Hyperspectral scattering image of MCF-7 cells incubated with bare AuNPs (upper, control). It is hard to differentiate the AuNP since they are buried within the scattering components of a cell. However, the optical clearing technique can remove the lipid droplets in cells as illustrated from the

signal of AuNP only (bottom, optical clearing) (b). Typical scattering spectra of AuNP (1) and cell components (2) marked in (a).

Section 2. Ultrafast Relaxation of a AuNP.

Different from the linear optical process which occurs on a AuNP under weak excitation of visible light, absorption of the intense and ultrafast light pulses, and the following relaxation process is a sophisticated procedure, which has been investigated for decades.^{5,6} For nanoscale AuNPs, there is a high density of empty electronic states at the Fermi level, (Figure 1) therefore the electrons have the high possibility to transit to the Fermi surface from or above the 5d band.

The response of AuNPs to the femtosecond pulses is a nonlinear process, which is depicted in Figure S2b. The absorption from the excitation pulses of the AuNP leads to oscillation of the conduction electrons, so called plasmons, which can be regarded as the superposition of many electron-hole pairs around the Fermi energy level. The dephasing of the plasmon through electron surface scattering leads to the absorption of photons, and this process is quite fast, in the range of 10 femtoseconds. (Figure S2a) The following recombination of electron and hole pairs can go through both nonradiative and radiative decay pathways. The radiative decay of the electron-hole pairs results in the fluorescence emission from the AuNPs with a typical time scale of few nanoseconds, so called fluorescence lifetime. However, in the last few decades, what is most investigated is the nonradiative decay pathway of electron-hole pairs of an illuminated AuNP.

Following the absorption of photons, the electron-hole pairs quickly lose the coherence and convert to individual electrons and holes over the conduction band. This procedure is called electron-electron cooling/scattering with a typical temporal range of 100 femtoseconds. Meanwhile, electrons also convert the energy to the lattice via the electron-phonon interaction with a temporal scale of few picoseconds. Therefore, the distribution of the electrons is affected by the vibration of phonons to the environmental lattice, which is in the range of 10-50 picoseconds. Eventually the electron-phonon coupling leads to the dissipation of thermal energy to the environment, which happens in the range of hundreds of picoseconds. These events discussed above are illustrated in Figure S2 with typical temporal scales noted.

These ultra-fast events can be detected by consecutive laser pulses. As discussed in the last paragraph, the excited electrons after absorbing the first laser pulse are mostly in the close vicinity of the Fermi energy level, above which all states are empty. Therefore, there is a high possibility for the excited electron to transit to higher energy levels after absorbing the second pulse. This procedure is named as transient absorption process, resulting in the energy loss of excitation beams within a short time range. And the first pulse is usually called pump, and the consecutive pulse is the probe.

The femtosecond ultrafast pump-probe spectroscopy is a standard tool to measure these events. Figure 2a shows the e-ph interaction with a typical time of 1.97 ps when fitting with an exponential decay curve, this value is usually called as the lifetime of carrier density of the metal nanoparticles. To measure the vibration of phonons and the heat transfer process, one needs to extend the temporal detection range to hundreds of picoseconds, as shown in Figure S2b. Damping of the phonons can be observed from the decay curves, which shows an increasing damping time from about 10 ps to 20 ps.

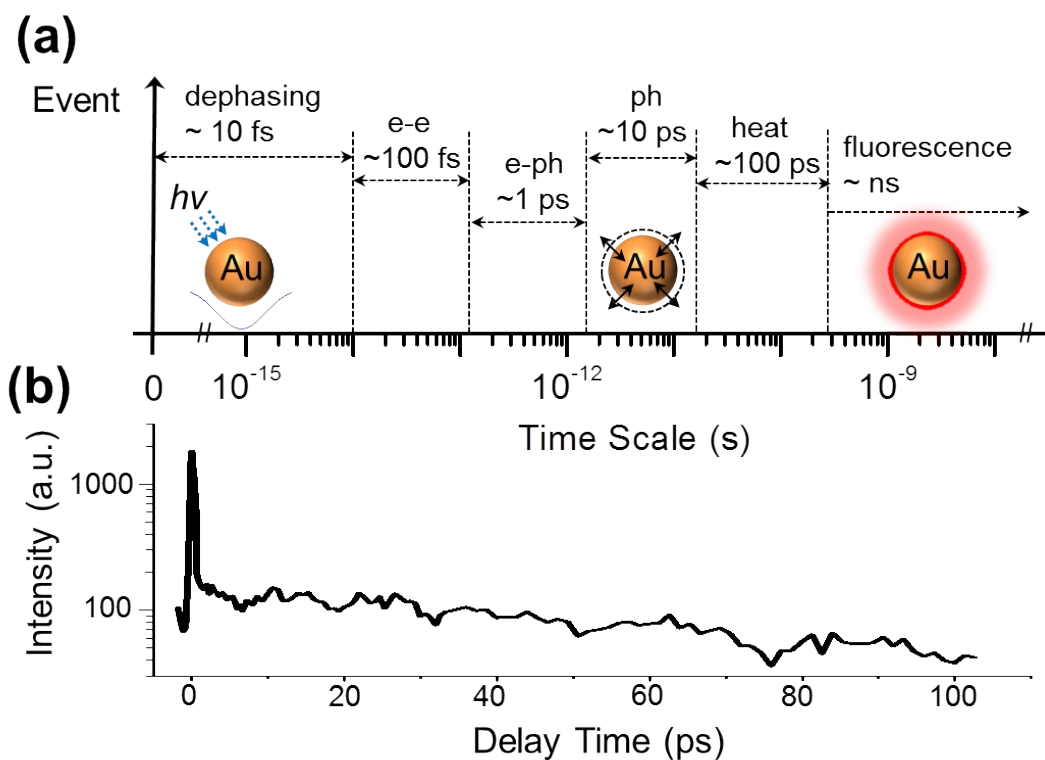


Figure S2. Response of a AuNP to ultrafast pulses. (a) Relaxation dynamics and the approximate time scales of AuNPs after absorbing a femtosecond laser pulses. e-e: electron-electron scattering; e-ph:

electron-phonon scattering; ph: phonon vibration. (b) Measured temporal response of the pump-probe signal with respect to the delay between pump and probe pulses. (c) Left: energy diagram of the transient absorption. Primary absorption of the pump beam happens between the ground state ($5d$) and the first state (E_1 , around the Fermi level), within the scattering time of electron and phonons (e-ph), the transient absorption of the probe beam happens between the two excited states (E_1 and E_2). Due to the empty states above the Fermi energy level, there is no saturation for this absorption process. Right: stimulated Raman process using the same pump-probe configuration. Absorption of the pump beam promotes the electron to a virtual excited state; the frequency of the probe beam matches well with the energy difference of the virtual state and vibration state, resulting in the stimulated emission of the probe beam.

Section 3. Materials and Methods.

Detailed Pump-Probe Microscopy Apparatus.

The scheme of the pump-probe scanning microscopy is depicted in Figure S3. A portion of the laser beam from femtosecond Ti:Sapphire laser (Chameleon Ultra, Coherent Inc.) working from 680 nm to 1080 nm with the pulse duration of 170 fs and repetition frequency of 80 MHz was used as pump beam, and the other part of the beam is directed to an optical parameter oscillator (OPO, Compact OPO, Coherent Inc.) to produce the synchronized probe beam, which has a tunable range from 1000 nm to 1500 nm and is independent of the pump beam. The pump beam and probe beam are spatially overlapped with a dichroic mirror (z1064rdc-sp, Chroma); the pulse trains of pump and probe beams are temporally overlapped with a home-made delay stage, and the delay time between pulse trains of pump and probe beams is tuned with a resolution of 30 fs. In our experiments, we set the pump beam working at 800 nm, and the probe beam is tuned from 1000 - 1200 nm within the OPO.

Before entering the microscope, the probe beam is modulated with the acoustic-optical modulator (AOM, 3080-122, Crystal Technology, LLC) which is driven by a sine function with frequency of 2.42 MHz to avoid the laser shot noise; and the first order diffraction beam was selected with the modulation depth of 100%. A half waveplate (10RP52-2, Newport) is located on the path of probe beam to ensure maximum signal.

Collimated pump and probe beams are free-space coupled to a modified laser scanning unit (C1, Nikon) which is hooked on an inverted microscope (IX71, Olympus); both beam are directed to the microscope by a short-pass dichroic mirror (680dcspxr, Chroma). Optical path is adjusted and proper

focus lens are chosen to ensure that the projection of the scanning mirror is on the back pupil of the water-immersed objective (UPlanApo/IR, Olympus; 1.2 NA, 60x), and the beam size fills the back-aperture of the objective. Light transmits through the sample and is collected with a 60x 1.3NA oil objective (UPlanSApo, Olympus) as condenser; care should be taken to ensure the conjugation of excitation objective and condenser. A telescope is used to project the scanning mirror onto the detector (photodiode) to avoid the movement of beam when scanning.

Since the probe beam was highly modulated, to avoid its influence on the detection of pump beam, three high OD bandpass filters (ET810/90m, Chroma) are used to block the probe beam. Transmitted pump beam is detected by a large-area photodiode (FDS1010, Thorlabs), with a reverse bias of 48 V. The output current is terminated with a 50 Ω resistor and then connected to a high-frequency lock-in amplifier (SRS844RF, Stanford Research Systems), which synchronized with the modulation frequency and is used to demodulate the pump-intensity. The in-phase component output of the lock-in amplifier is fed into the input of control unit of the scanners. The pump-probe microscopy functions in a beam-scanning mode. To avoid the cross talk of pixels, pixel dwell time (32.00 μ s) is selected to be larger than the reciprocal of the modulation frequency (2.42 MHz). The images are processed in ImageJ.

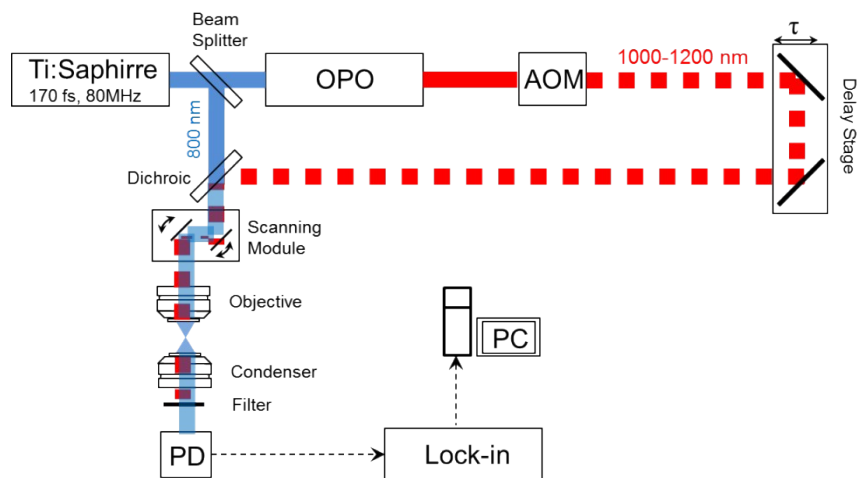


Figure S3. Schematic illustration of the pump-probe setup. OPO: optical parameter oscillator; AOM: acoustic-optical modulator; Lock-in: lock-in amplifier; PD: photodiode; PC: personal computer.

Oligonucleotide-AuNP Conjugate.

30 nm gold nanoparticles (AuNP) were synthesized in our lab according to prior literatures.⁷ For a good monodispersibility and flexible conjugation, the surface of the AuNPs were chemically modified with a layer of amino group by (3-Aminopropyl) triethoxysilane (APTES, Sigma) treatment.⁸ To link modified AuNPs to single strand oligonucleotides, AuNPs were further treated with the crosslinker SMCC (Sigma), to produce maleimide-terminated AuNPs. Oligonucleotide with the complementary sequence to the targeted mRNA was purchased from IDT-DNA, Inc. Its sequence is listed as AGAACTGAGATGAGGTGGGGttttttttC3-3'-/ThiolM. Finally the AuNPs were incubated with reduced oligonucleotides at 60 °C for 1 h. Details of these procedures can be found in our previous reports.^{8,9}

Cell Culture and Incubation with mRNA Probes.

MCF-7 and SK-BR-3 cells were cultured on coverslips in Dulbecco's Modified Eagle's Medium (DMEM/F12) medium supplemented with 10% fetal bovine serum and 1% antibiotics at 37 °C in an atmosphere of 5% CO₂. Upon reaching ~70% confluence, cells were washed by PBS three times, and fixed by 4% paraformaldehyde (PFA) for 15 min. Cells were rinsed again before being permeabilized by 0.1% Triton-X for 1 hour. Finally cells were washed before incubation with oligonucleotide-AuNP probes; the incubation was performed at room temperature overnight in PBS, and washed with PBS before imaging.

Fluorescence *In Situ* Hybridization.

As a control for our mRNA quantification using AuNPs with transient absorption microscopy, we also performed the standard FISH experiment to quantify Her2 mRNA in SK-BR-3, and MCF-7 cells. Commercial Stellaris[®] FISH probes which include Quasar[®] 570 dye (SMF-2010-1, Biosearch Technologies, Inc.) as reporters and oligonucleotides recognizing Her2 (ERBB2) mRNA were hybridized to SK-BR-3 and MCF-7, following manufacturer's instructions available online at www.biosearchtech.com/stellarisprotocols with minor modifications. MCF-7 and SK-BR-3 cells were fixed with 4% paraformaldehyde, followed by permeabilization with 70% ethanol for 1 hour at 4°C.

Stellaris® RNA FISH probes of 125 nM were incubated with cells in hybridization buffer containing 100 mg/ml dextran sulfate, 10% formamide, and 2× SSC overnight in the dark at 37 °C. The sample slides were then washed with 10% formamide in 2× SSC and counterstained with DAPI. After final washing, the sample was mounted onto a clean slide using Vectashield mounting medium and sealed by nail polish for imaging. The RNA and nuclei imaging were performed with confocal scanning microscopy (LSM 710, Zeiss); laser lines 405 nm and 561 nm are applied as excitations for DAPI imaging and mRNA imaging, respectively. Her2 mRNA was quantified with the plugin “ITCN” in ImageJ.

Tissue Processing.

Cancer tissue slides and normal tissue slides from Breast cancer patients were gifted from Dr. Kurt B. Hodges from Indiana University, School of Medicine. Tissue slides were first deparaffinized by immersing in xylenes (Histological grade, Fisher Scientific) three times, and then were rehydrated by graded ethanol (Pharmco-AAPER) gradually. After that, the tissue was treated with a mixture of Tris-Buffered Saline (BioRad) and Tween 20 (TBST, Sigma) and then incubated in an environment of sodium citrate buffer at 100 °C for 30 min. Finally the slides were incubated with oligonucleotide-AuNP conjugates overnight to ensure their binding to the mRNA. All slides were washed with PBS three times before performing the imaging.

Section 4. Results.

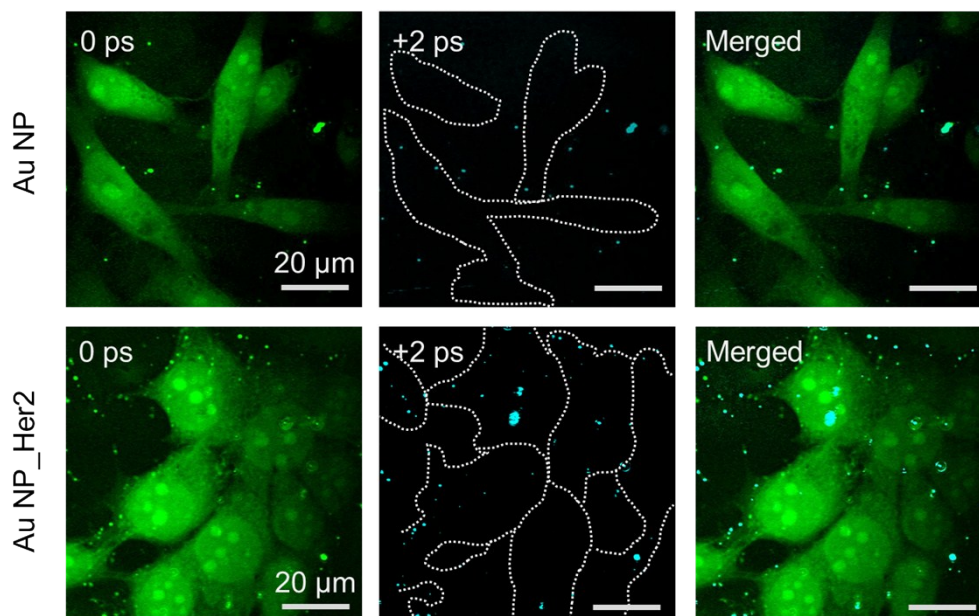


Figure S4. Pump-probe images of MCF-7 cells incubated with bare AuNPs (upper) and AuNP_Her2 conjugates (bottom) showing the binding specificity of the conjugates. Left row is the SRS image with 0 ps delay; middle row is the TAM image with 2 ps delay, white dashed lines indicate the boundary of cells; right row is the merged image of both channels. Very few AuNPs can be observed within the cells for the nonspecific binding of bare AuNPs.

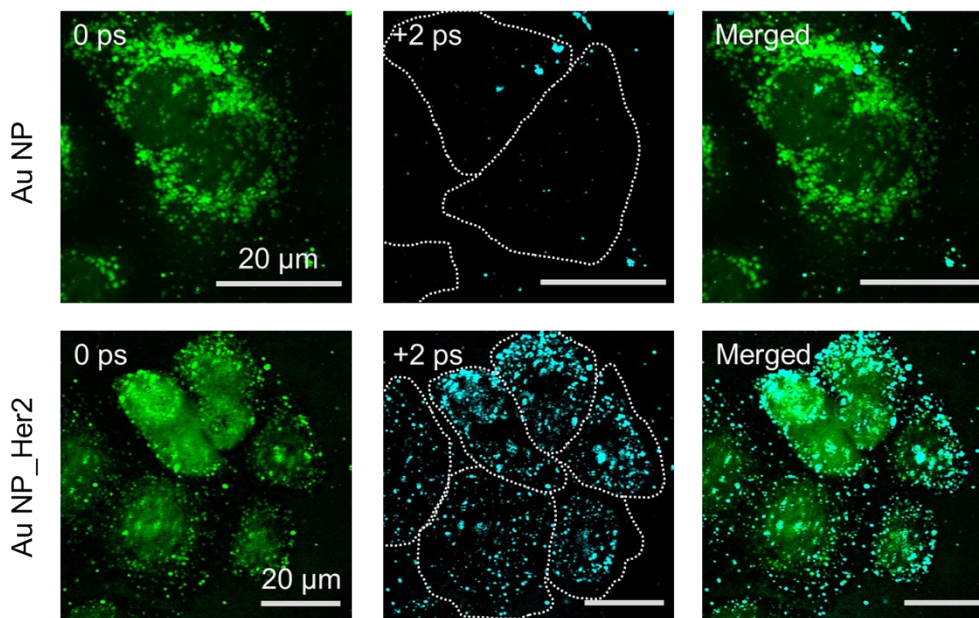


Figure S5. Pump-probe images of SK-BR-3 cells incubated with bare AuNPs (upper) and AuNP_Her2 conjugates (bottom) showing the binding specificity of the conjugates.

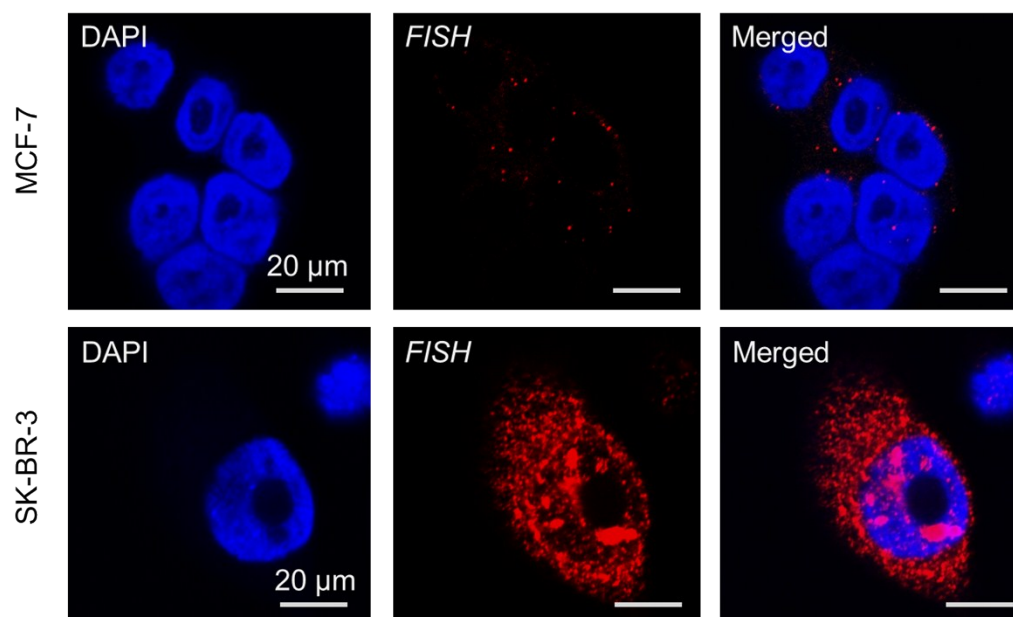


Figure S6. Confocal images of Her2 mRNA in MCF-7 cells (upper) and SK-BR-3 cells (bottom) using the standard FISH approach. Left row (blue) is the DAPI channel showing the cell nucleus, middle row (red) is the FISH channel showing the localizations of Her2 mRNA. The right row is the merged images.

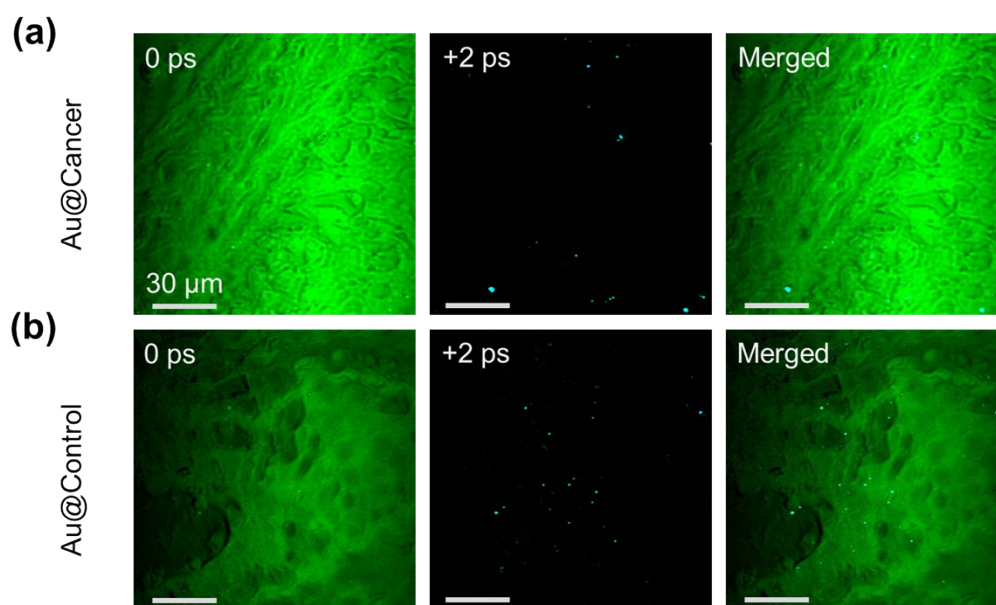


Figure S7. Pump-probe images of breast cancer tissue (upper) and normal tissue (bottom) incubated with bare AuNPs as negative control of Figure 5.

References

1. Lee, K.; Drachev, V.; Irudayaraj, J. DNA-Gold Nanoparticle Networks Grown at Cell Surface Marker Sites: Diagnostics of Cancer Stem Cells. *ACS Nano* **2011**, *5*, 2109–2117.
2. Lee, K.; Irudayaraj, J. Correct spectral conversion between surface-enhanced Raman and plasmon resonance scattering from nanoparticle dimers for single-molecule detection. *Small* **2012**, *9*, 1106–1115.
3. Lee, K. C.; Cui, Y.; Lee, L. P.; Irudayaraj, J. Quantitative Imaging of Single mRNA Splice Variants in Living Cells. *Nat. Nanotechnol.* **2014**, *9*, 474–480.
4. Cui, Y.; Wang, X.; Ren, W.; Liu, J.; and Irudayaraj, J. Optical clearing delivers ultrasensitive hyperspectral dark-field imaging for single-cell evaluation. *ACS Nano*, **2016**, *10*, 3132-3143.
5. Zijlstra, P.; Orrit, M. Single Metal Nanoparticles: Optical Detection, Spectroscopy and Applications. *Rep. Prog. Phys.* **2011**, *74*, 106401-106456.
6. Hartland, G. V. Optical Studies of Dynamics in Noble Metal Nanostructures. *Chem. Reviews* **2011**, *111*, 3858-3887.
7. Zhou, J.; Ralston, J.; Sedev, R.; Beattie, D. A. Functionalized Gold Nanoparticles: Synthesis, Structure and Colloid Stability. *J. Coll. Inter. Sci.* **2009**, *331*, 251-262.
8. Liu, J.; Cho, I.; Cui, Y.; Irudayaraj, J. Second Harmonic Super-resolution Microscopy for Quantification of mRNA at Single Copy Sensitivity. *ACS Nano* **2014**, *8*, 12418-12427.
9. Sun, L.; Irudayaraj, J. Quantitative Surface-Enhanced Raman for Gene Expression Estimation. *Biophys. J.* **2009**, *96*, 4709–4716.